Materials & Design 264 (2026) 115724

Contents lists available at ScienceDirect

Materials & Design

journal homepage: www.elsevier.com/locate/matdes

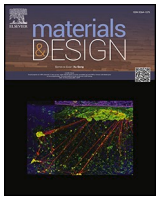

# Thermo-mechanical simulation of microstructure and texture evolution in flat-strip extrusion of Al–Mg–Si-Cu alloy

Sri Saran Gunasekaran [a], E. Bagherpour [a], Chrysoula Tzileroglou [b], Carla Barbatti [b,c], Chamini L. Mendis [a,*]

[a] Brunel Centre for Advanced Solidification Technology (BCAST), Brunel University of London, Uxbridge, UK
[b] Constellium University Technology Centre, Brunel University of London, Uxbridge, UK
[c] Constellium Technology Centre (C-TEC), Voreppe, France

ARTICLE INFO

*Keywords:*
Thermo-mechanical simulation
Hot Extrusion
Al-Mg-Si alloy
Gleeble
Deformation mode
Microstructure development

ABSTRACT

Enhancing the mechanical properties of aluminium extrusions has been a subject of industrial interest for many years. Conventional approaches focused on tuning the extrusion parameters and have established correlations with the final microstructure, but a mechanistic understanding of how microstructures evolve during extrusion remains limited. To address this, a physical simulation methodology was developed for flat-strip extrusion, allowing detailed examination of microstructural evolution and providing a pathway for future microstructure and texture design. Currently, this work focuses on physically reproducing the microstructure and texture of the central region of an industrially extruded Al-Mg-Si-Cu flat strip by replicating its strain path. The microstructures and textures simulated using a Gleeble thermomechanical simulator were compared with industrial extrusion to assess the fidelity of the approach. The results demonstrate that the simulation at 580 °C reproduced elongated grain shape, dominant < 112>//ED texture and morphology of the intermetallics which are the key features of strip extrusion. Quantitative comparisons revealed close agreement in microstructure and texture, with limited differences. Overall, the study confirms that this method provides a reliable framework for capturing the deformation conditions of flat-strip extrusion. Beyond validation, the present approach provides a versatile platform for future studies aimed at investigating the onset and progression of recrystallisation, second-phase particle evolution, and strain path effects through systematic characterisation of microstructure at intermediate strain levels.

## 1. Introduction

Extrusion is one of the most important forming processes used extensively to produce structural components especially in the automotive sector applications including chassis, crash management systems, body structures and heat exchangers [1,2]. Amongst the various aluminium alloys, 6xxx series (Al-Mg-Si) alloys are extensively used in extruded form due to their excellent formability and high specific strength. The final performance of extruded products is strongly governed by the end microstructure which develops dynamically during hot extrusion. This includes elongation and distortion of grains, fragmentation of intermetallics, substructure formation, recrystallisation, and crystallographic reorientation. These transformations are strongly influenced by the interplay of strain, strain rate, temperature and deformation mode along the material flow path. While many studies have linked extrusion parameters to microstructure and properties [3–6], a clear mechanistic understanding of how microstructures evolve dynamically throughout the entire extrusion process remains incomplete. The need to understand microstructure evolution in real time is essential not only for understanding extrusion but also for controlling it for achieving better mechanical properties.

Industrial extrusion provides little opportunity to observe microstructural transitions inside the die, as extracting partially extruded billets from large-scale setup is challenging. To overcome this limitation, laboratory-scale extrusion setups have been developed, which allow investigations of material flow and microstructure evolution by sectioning partially extruded billets. For instance, number of studies [7–9] have examined the formation of surface microstructures in bar extrudates, where shear and strain are highest, while [10] focused on dynamic grain flow and the influence of extrusion parameters on the

* Corresponding author.
*E-mail address:* chamini.mendis@brunel.ac.uk (C.L. Mendis).

https://doi.org/10.1016/j.matdes.2026.115724
Received 19 December 2025; Received in revised form 22 January 2026; Accepted 23 February 2026
Available online 26 February 2026

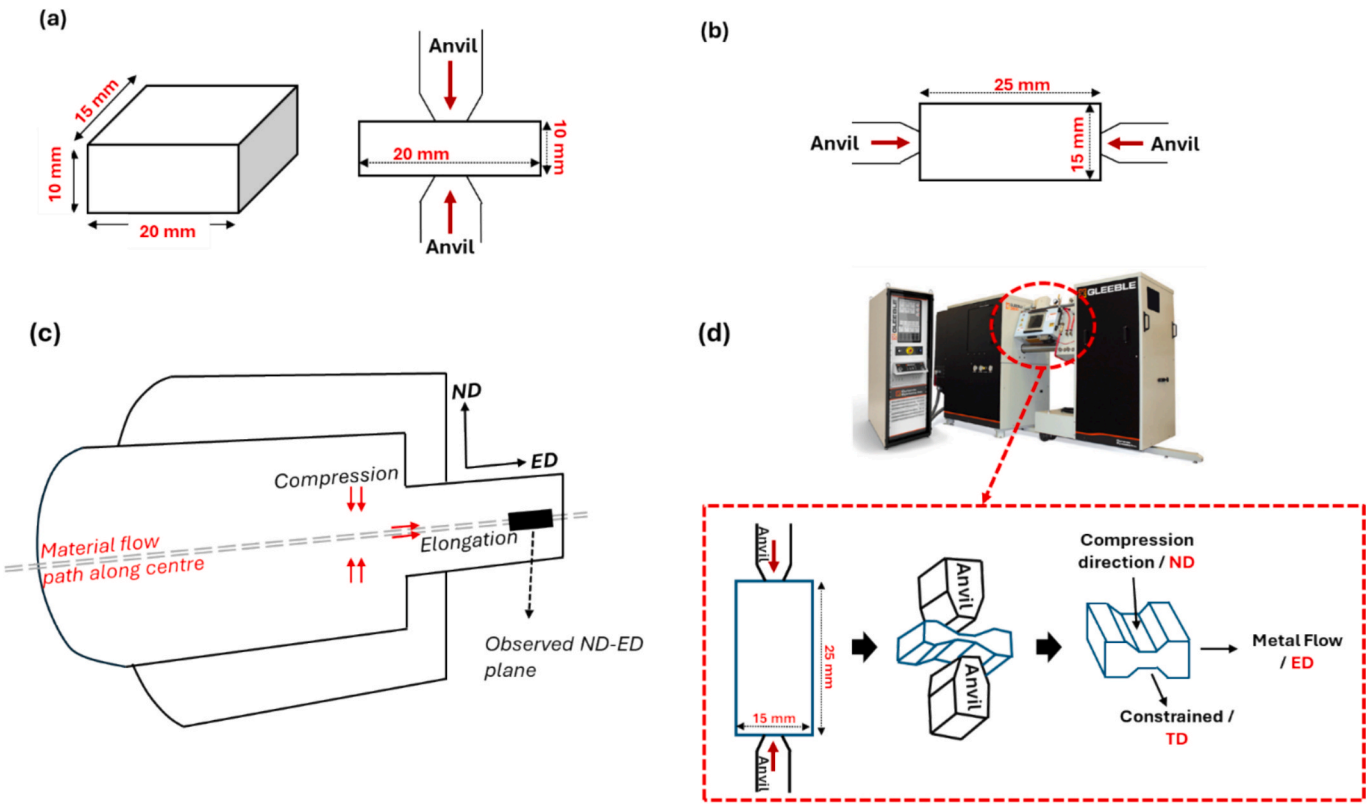


**Fig. 1.** (a) Standard plane strain sample geometry and corresponding loading conditions (b) modified sample geometry to achieve industrial strain and loading conditions (c) Schematic representation of the stress states experienced during central portion of billet during extrusion (d) Schematic of deformation simulated using Gleeble and sampling method similar to industrial extrusion.

microstructure and texture of A6N01 (equivalent to alloy 6005A) alloy bar geometries. In addition, Araki et al. [11] investigated the effect of alloy composition on recrystallisation texture formation in porthole die extrusions. Although these laboratory setups provide valuable insights, they are constrained by fixed die geometries and offer limited flexibility to systematically vary strain paths. Numerical approaches, including finite element modelling (FEM) which is constitutive equations based, have advanced significantly and provide useful predictions at various stress–strain states during processing. For example, [12] combined laboratory-scale extrusion trials with FEM to predict recrystallised grain size distributions in AA6060, while [13] developed phenomenological models for grain thinning, elongation, and pinch-off in AA6082 and AA7020. Furthermore, several other studies [14–21] have employed crystal plasticity-based FEM to track macro-texture evolution during extrusion.

Previous FEM studies and experimental observations provide valuable guidance on the deformation mode experienced by a material flow path. Fylkesnes et al. [15] and Manik et al. [16] predicted the deformation mode of the flat strip extrusion at 350 °C reported that, in the centre region of extrudate the grains are compressed along the normal direction (ND), stretched along the extrusion direction (ED) and constrained along the transverse direction (TD). Both the authors conclude that deformation mode transitions from stretching before die exit to plane strain compression at the exit, with minimal shear contribution in the central region of the flat strip. Similarly, Aukrust et al.[19] also observed plane strain deformation at 520 °C for a material path flowing along the centre. In contrast, Zhou et al.[22] has predicted that, shear deformation dominates in the centre region rather than the stretching/compression above 500 °C, as the friction stress increases with the increase in temperature. A relevant comparison can be drawn from hot rolling, where the mid-plane is widely recognised to undergo plane strain compression, producing grains with a β-fibre texture [23–25] which is similar to that observed in flat strip extrusions [16,26]. Moreover, the pancake-shaped grains observed in rolled and post-extrusion microstructures [3] further support the presence of plane strain compression rather than simple shear. Chen et al. [7] physically simulated the surface texture of the AA3003 flat strip at 350C using the torsion test. Although quantitative comparisons have not been discussed but the qualitative comparisons seem to agree.

In summary, most numerical simulation studies provide evolution of macro textures and lacked detailed microstructural models. Dynamic recovery and recrystallisation are inherently complex metallurgical phenomena that cannot be fully or accurately captured using numerical models. Experimental investigations using laboratory-scale extrusion setups have addressed some of these limitations, but studying alternative strain paths requires frequent changes of dies, which reduces flexibility. For instance, hot rolling research have already advanced their potential by replicating industrial strain paths and thermal histories by using thermomechanical simulators [27,28]. Extending this concept to extrusion could provide a pathway to systematically investigate and even tailor microstructure development. While most extrusion studies have focused on bar geometries and shear-dominated regions (surface), the microstructure development of flat-strip extrudates has remained largely unexplored. This region not only experiences distinct deformation modes but also constitutes most of the load-bearing volume, making it critical to understand the microstructural evolution for better mechanical performance.

To address this gap, the present study aims to develop a physical simulation methodology using Gleeble thermomechanical simulator to physically replicate the strain path of flat-strip extrusion, focusing specifically on the centre region of the extrudate. In this study, industrial strain, strain rate, and thermal conditions are reproduced in small-volume samples, and the methodology is validated against microstructures observed in industrial extrudates using electron backscatter

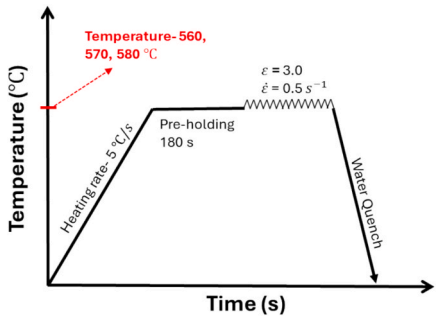


**Fig. 2.** Thermal cycle diagram used in the physical simulation.

diffraction (EBSD) and scanning electron microscopy (SEM). This methodology in future provides a potential pathway for understanding the dynamic sequence of grain shape change, recovery, recrystallisation, and texture development under extrusion-relevant conditions by interrupting experiment at selected strain levels. Moreover, it offers the flexibility to deliberately modify strain paths, enabling systematic tailoring of microstructure and texture during extrusion to optimise material performance.

## 2. Materials and Methods

The industrial reference material used in this work is extruded flat strip of an Al-Mg-Si-Cu alloy, supplied by Constellium and processed at the Advanced Metal Casting Centre, Brunel University of London. The alloy was first cast as a DC billet and subsequently homogenised according to the standard industrial procedure prior to hot working. The extrusion is conducted at a total equivalent strain of 3 at a temperature range between 520 and 560 °C and strain rate range of 3–5 $s^{-1}$.

For the thermo-mechanical simulation, billets with the same alloy chemistry and homogenisation treatment were obtained. This ensured comparable initial grain size, second phase particles size and distribution for simulation and industrial extrusion. Only the inner 50% of the billet radius is considered for machining the samples in this simulation, as this region primarily contributes to the central portion of the extrudate [16].

The thermo-mechanical simulation of the flat strip extrusion was conducted using a Gleeble-3800 GTC system equipped with a Hydrawedge module to replicate the extrusion strain path. In plane strain compression achieving the industrial-scale strain of 3 is not achievable using the standard method as shown in Fig. 1a. To execute the required strain, the sample length was extended to 25 mm with loading applied along this axis. To ensure deformation constraint along the lateral axis (TD), the thickness and width of the specimen are also increased to 15 mm and 20 mm, respectively (Fig. 1b).

The industrial extrusion parameters are used as a baseline in the physical simulation, as represented in the thermal cycle diagram (Fig. 2). Simulation conducted at industrial parameters either at 560 °C or strain rate of 3/s resulted in a deformation dominated texture and absence of main recrystallisation components (see supplementary section for more information). Direct application of these parameters in the Gleeble is not feasible due to the reduced sample size, which limits adiabatic heating and alters the effective thermomechanical response. Therefore, the deformation conditions were adjusted to achieve thermomechanical similarity with industrial extrusion. The simulation is conducted using a preheating duration of 180 s followed by deformation at three different temperatures (560, 570 and 580 °C) at a lower strain rate of 0.5/s that industrial rate. The slightly elevated deformation temperatures were selected to compensate for the absence of adiabatic heating in the smaller Gleeble samples. In addition to thermal effects, the strain-rate history in industrial extrusion is inherently non-uniform, evolving continuously from relatively low values in the container to peak values near the die exit. In the Gleeble, this complex strain-rate path must be simplified to a single constant value. Using a constant high industrial strain rate under such simplified conditions overemphasises severe deformation, promotes excessive work hardening, and suppresses recovery controlled recrystallisation mechanisms. Consequently, a reduced constant strain rate was selected to approximate the effective average strain-rate history experienced by the billet core rather than the peak industrial value.

The extruded samples were characterised through the thickness along the ND–ED plane. For the physically simulated samples when compressed axially (ND) the material was forced to flow vertically (ED),

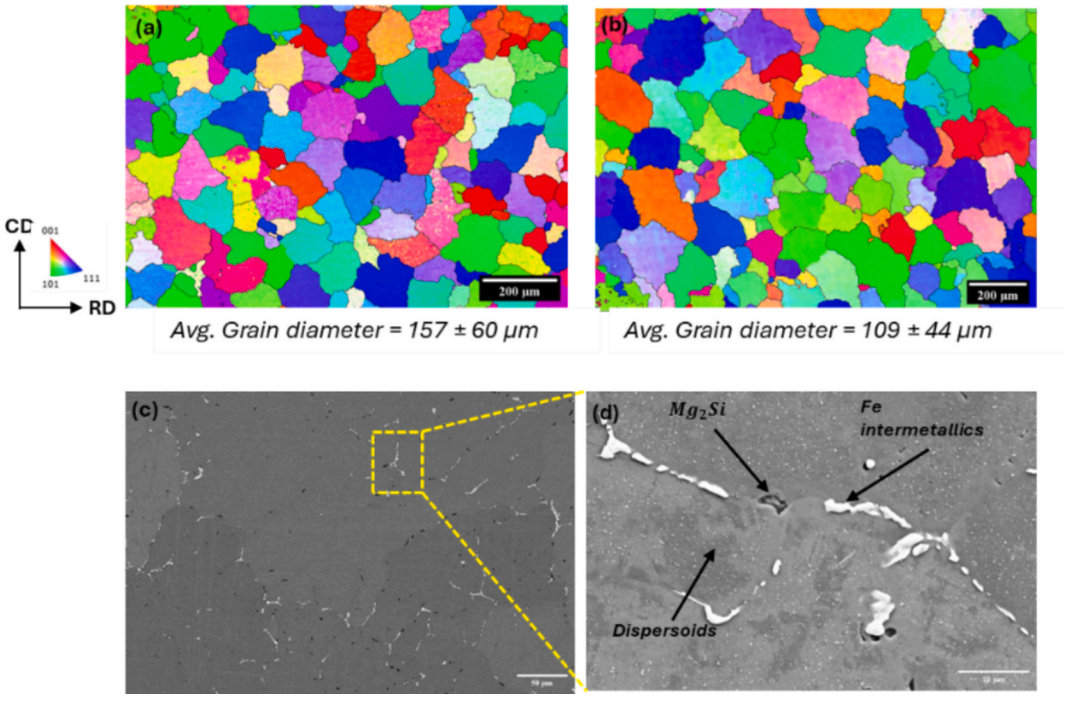


**Fig. 3.** IPF maps of homogenised billet at centre (a) and half radius (b), along with SEM images (c, d) illustrating second phase particles.

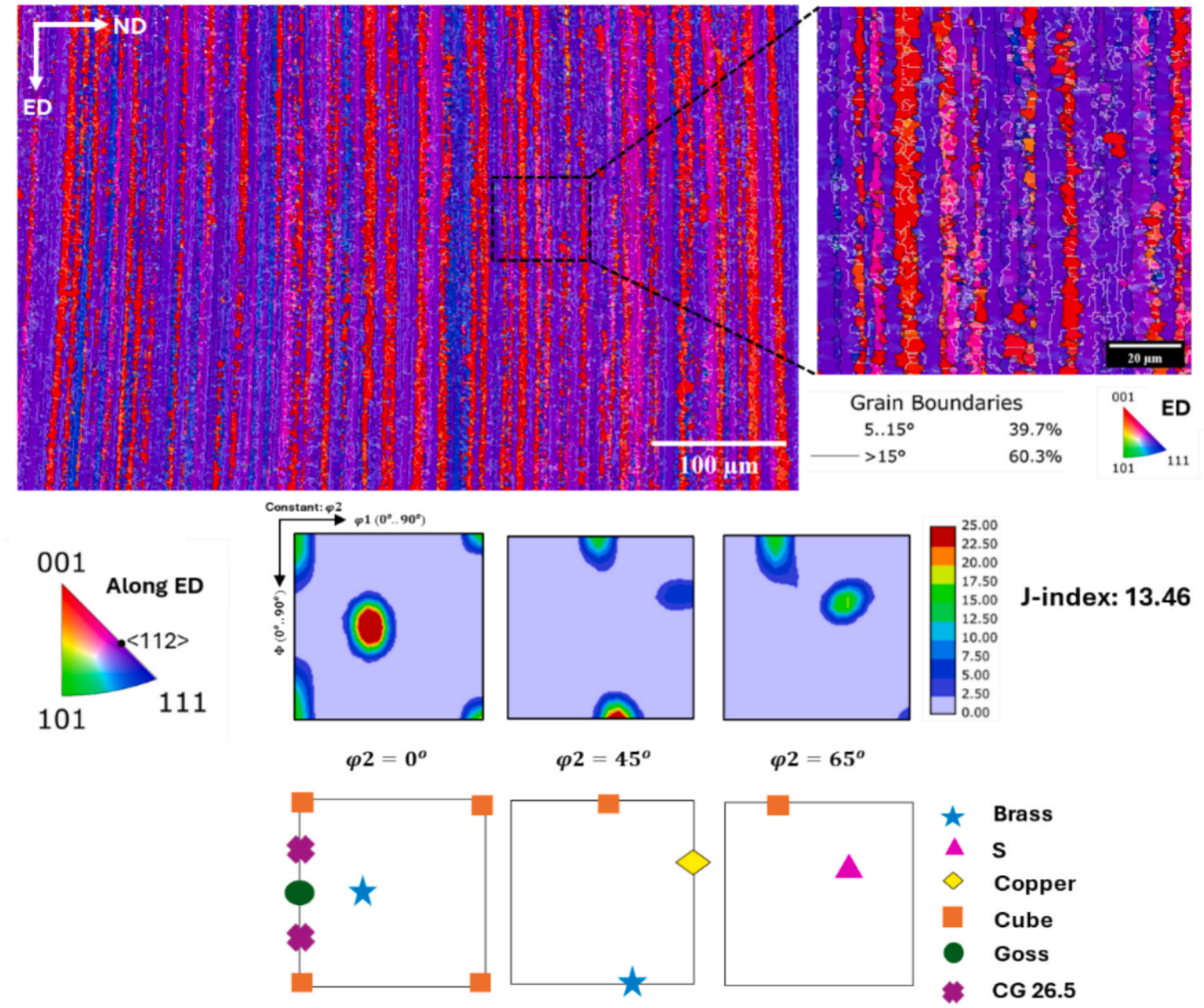


**Fig. 4.** IPF map, inverse pole figure and ODF component observed in the industrially extruded flat strip.

and lateral direction (TD) is highly constrained with only minimal lateral material flow (limited to approximately 2 mm). The sample orientation and sectioning plane used in the simulation were carefully aligned to replicate the industrial extrusion orientation, as illustrated in Fig. 1.

Sample preparation involved standard mechanical grinding and polishing, followed by final polishing with colloidal silica. For optical microscopy the sample is anodised using Barker's reagent at 20 V for 2 mins to reveal the grain boundaries. For SEM analysis, the samples are electropolished using 30% nitric–methanol solution at 16 V and −30 °C for 60 s. Microstructural characterisation was carried out using a ThermoFisher Apreo 2 SEM under an accelerating voltage of 10 kV and a beam current of 1 nA. The EBSD were acquired (step size- 0.15 to 0.5 µm) using the Symmetry S2 detector at an accelerating voltage of 20 kV, beam current of 6.4 nA and processed using AZtecCrystal software. The data points have been cleaned no more than 5% to maintain originality. The texture map in this study is represented in the ED-TD plane and grain boundaries with misorientation angles between 5 ° and 15 ° were classified as Low Angle Grain Boundaries (LAGBs), while boundaries with misorientations greater than 15 ° were considered High Angle Grain Boundaries (HAGBs).

For analysis of intermetallic particles, SEM images used were acquired from the central region of the samples and processed using MATLAB to quantify particle area and aspect ratio. For each condition, three micrographs were analysed to ensure statistical reliability. Segmentation was performed by converting the images to binary format using a fixed global intensity threshold of 0.65. Intermetallics touching the image borders and features smaller than 8 pixels (attributed to noise from dispersoids) were removed. Particle morphology was quantified using the normalized aspect ratio, defined as the ratio of the minor axis to the major axis. The same parameters were applied to maintain consistency for all the analysis.

## 3. Results and Discussion

### 3.1. Initial microstructure

#### 3.1.1. Homogenised billet

Fig. 3 shows the microstructures at the centre and half-radius of the billet in the homogenised condition. EBSD analysis confirms that the grains are largely equiaxed, with an average grain diameter of 157 ± 60 µm at the centre and 109 ± 44 µm at the half-radius. The variation in grain size reflects the thermal gradient during homogenisation, leading to slightly coarser grains in the centre. The pole figures further indicate that the texture is completely random, confirming the absence of any crystallographic orientation preference in the homogenised state. SEM imaging reveals the presence of Fe-rich intermetallics, predominantly located along grain boundaries along with $Mg_2Si$ particles. Finely dispersed thermally stable dispersoids are distributed within the grains, which will contribute to microstructural stability during subsequent deformation. Overall, the homogenised billet exhibits a uniform and well-equiaxed grain morphology with evenly distributed secondary

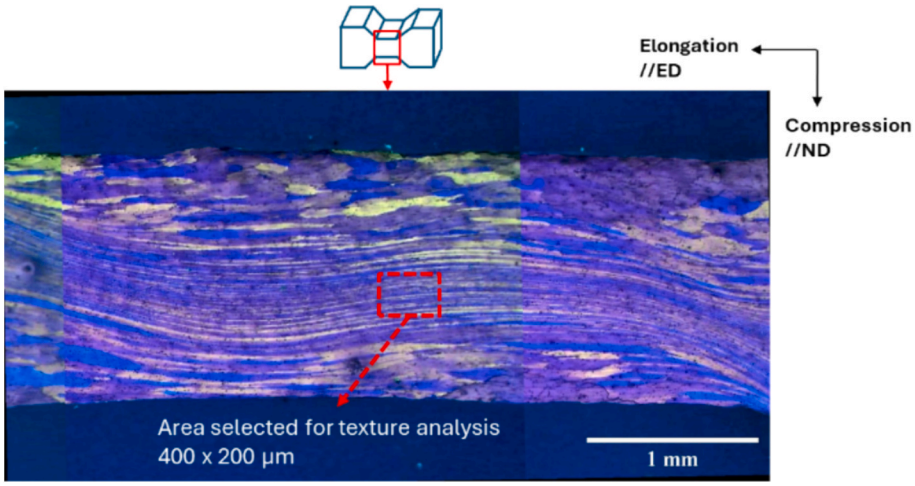


**Fig. 5.** Etched longitudinal cross-section of the sample simulated at 560 °C, imaged using an optical microscope.

phases, providing the initial state for both physical simulation and extrusion.

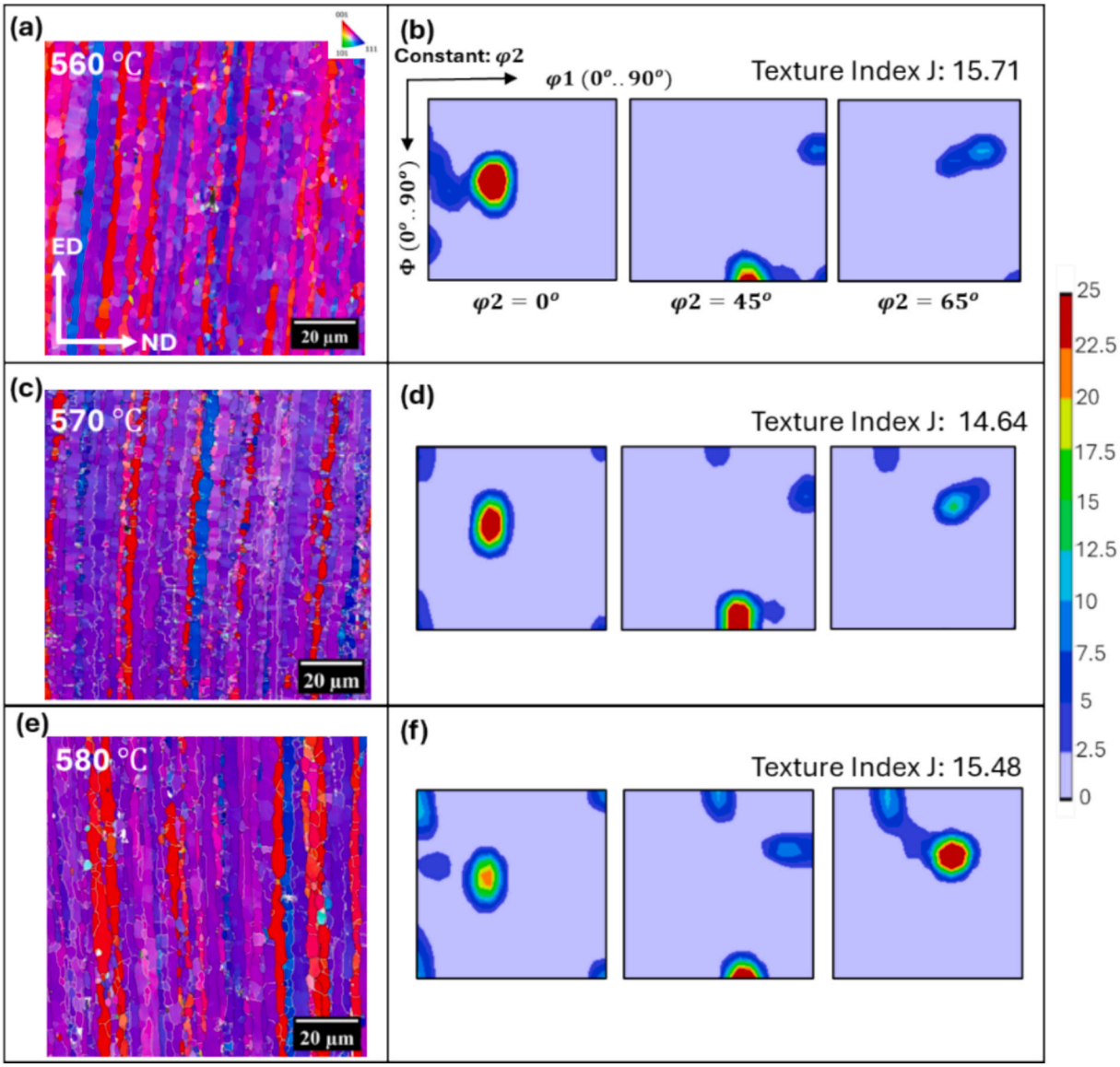


**Fig. 6.** IPF map (a, c, e) and ODF plots (b, d f) of the simulated samples processed at 560 °C (a, b), 570 °C (c, d), and 580 °C (e, f).

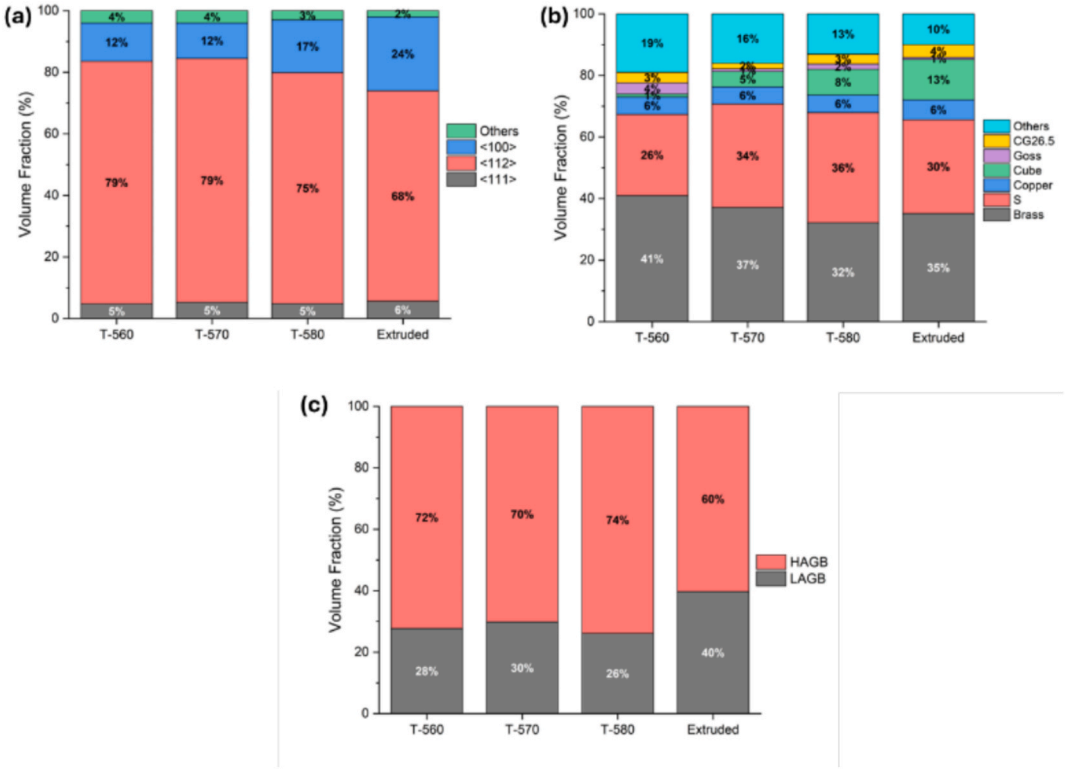


**Fig. 7.** (a)Evolution of the principal texture fibre (b) corresponding texture components derived from ODF and (c) grain boundary fractions (LAGB = 5 °-15 °, HAGB= >15 °) in the simulated and extruded samples.

### 3.1.2. *Reference sample- Extruded*

To enable comparison with the physical simulation, EBSD was carried out on an industrially extruded flat-strip sample. Since the purpose of this study is to replicate only the centre region of the strip, the EBSD analysis was also restricted to this location. This ensures a direct and meaningful comparison between the industrial and simulated conditions. The inverse pole figure (IPF) map in Fig. 4 represents the microstructure in the T4 state. The initially globular grains have been severely compressed along the normal direction (ND) and elongated along the extrusion direction (ED), reflecting the intense material flow imposed during extrusion. The average grain thickness of 2.69 ± 1.48 μm along ND indicates this flattening effect, highlighting the severity of compression in the central zone.

The elongated grains form a pronounced dual-fibre texture dominated by < 112>//ED and < 100>//ED components, while < 111>// ED orientations are weak. The corresponding orientation distribution function (ODF) confirms the presence of typical plane-strain deformation components such as Brass {110} < 112>, S {123} < 634>, and Copper {112} < 111 > . Among these, Brass and S are most intense, consistent with the strong < 112 > fibre, whereas the Copper component is weaker due to the limited < 111>//ED fibre. In addition to elongated grains, a fraction of fragmented grains is observed, signifying the operation of multiple dynamic recrystallisation (DRX) mechanisms. The recrystallisation texture is primarily dominated by the Cube component {001} < 100>, accompanied by a minor presence of the CG 26.5 component {021} < 100 > . Grain boundary misorientation analysis reveals 39.7% LAGB and 60.3% HAGB, reflecting a combination of substructure development and recrystallised grain formation.

## 3.2. *Microstructure evolution during physical simulation*

The homogenised billet samples were subjected to plane strain compression to replicate the strain path of flat-strip extrusion. For this study, only the material directly deformed in contact with the anvils was considered, as shown in Fig. 5. The etched cross-section reveals a heterogeneous strain distribution across the sample thickness. Such heterogeneity is consistent with previous study [29] and originates primarily from interfacial friction at the specimen–anvil contact surfaces as well as local temperature gradients. Despite the heterogeneous strain distribution, the extended sample length (25 mm) along the loading axis produces additional elongation along the perpendicular direction, while deformation remains constrained along the lateral direction. This flow condition closely mimics the material behaviour in flat-strip extrusion, where the billet is compressed in thickness, stretched in the extrusion direction, and restricted laterally by die walls. As a result, the centre zone in simulation develops a clear grain flow pattern perpendicular to ND. Huang et al. [30]and Poletti at al [31] has shown that the centre region of the sample experiences homogeneous strain distribution with FEM simulation. In this study, the central region is therefore taken as the most reliable representation of extrusion-induced microstructural evolution and was selected for further EBSD analysis.

Fig. 6 presents the IPF maps and ODFs taken from the centre region for the samples simulated at various temperatures with constant strain rate of 0.5/s. At all investigated temperatures the microstructure shows very elongated grains aligned along the flow direction. This appearance further complements the predominant compression acting along the central portion of the sample and the grains elongate along the perpendicular direction as macroscopically observed in Fig. 5. Additionally, small and fragmented grains are also distributed heterogeneously throughout the microstructure like in extruded sample.

The crystallographic texture at all investigated temperatures is strongly dominated by the < 112>//ED fibre, which accounts for 75–79% of the total fraction (Fig. 6). The < 111>//ED component remains consistently weak at 5% across all temperatures, while the < 100>//ED fibre shows a notable temperature dependence. At 560 °C (T-560) and 570 °C (T-570), <100>//ED is limited to 12% of the texture and increases to 17% at 580 °C (T-580). The ODF analysis (Fig. 6) confirms the presence of typical plane-strain deformation components

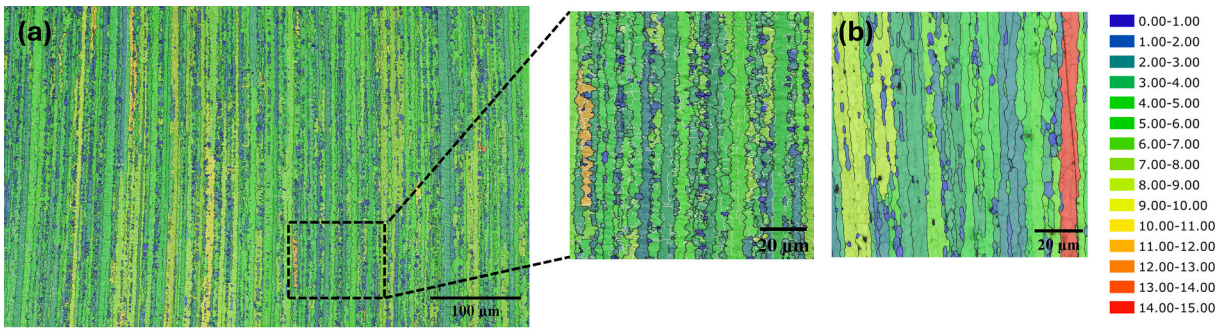


(c)

| | Extruded | T-580 |
|---|---|---|
| **Recrystallised (GOS 0-2)** | 5.8% | 6.5% |
| **Sub-structured (GOS 2-5)** | 48.1% | 56% |
| **Deformed (GOS >5)** | 45.9% | 37.7% |

**Fig. 8.** Grain orientation spread maps for the industrial extruded sample (a) and simulated T-580 sample (b) along with the table of recrystallised, sub-structured and deformation fraction of grains (c).

(Brass, S, and Copper) across all conditions. Brass exhibits a steady decrease in volume fraction from 41% at 560 °C to 32% at 580 °C, while the S component strengthens significantly, increasing from 26% to 36%. The Copper component remains nearly unchanged at 6%, consistent with the stability of the < 111>//ED fibre.

Importantly, recrystallisation-related components show a strong temperature dependence (Fig. 6 and Fig. 7). At 560 °C, the < 100>//ED fibre primarily contributes to Goss and CG 26.5 orientations. However, as the deformation temperature increases to 570 °C, the Goss orientation disappears, and the Cube component begins to form. At 580 °C, the < 100>//ED fibre fraction intensifies further, accompanied by an increase in the cube component, while CG 26.5 remains stable across all temperatures. This progression highlights a clear transition from Goss dominated texture at 560 °C to Cube dominated texture at 580 °C.

Fig. 7 illustrates the changes in the grain boundary fractions with varying temperatures. It can be observed that the fraction of LAGB and HAGB largely remains consistent. This indicates that the deformation temperature has limited influence on grain boundary character. Overall, these results show that while the deformation texture (<112>//ED-Brass and S components) remains predominant across all conditions, the balance between Goss and Cube strongly depends on temperature in this simulation.

### 3.3. Comparison between extrusion and physical simulation

For a physical simulation to be a reliable predictive tool, the results are validated against real-world industrial extrusion. The physical simulation results exhibit a strong qualitative agreement with the deformation microstructure and texture observed in the extruded sample. The main difference appears in the recrystallisation textures, as cube is the primary component formed in extrusion followed by the CG 26.5. As shown in the Supplementary Information, simulations performed using industrial deformation temperatures and strain rates (560 °C-3/s strain rate) did not yield Cube component, despite increasing the temperature (580 °C-3/s strain rate) compared to industrial condition. This indicates that direct replication of industrial parameters in the Gleeble does not adequately capture the recrystallisation behaviour.

In contrast, simulations at lower deformation temperatures and reduced strain rate (560 °C-0.5/s strain rate) produce a dominant Goss component, with the transition towards cube orientation occurring above 570 °C. The simulation at 580 °C yields a cube fraction most comparable to industrial extrusion, highlighting the sensitivity of recrystallisation textures to deformation temperature. This difference originates from the thermal environment of industrial extrusion, where the local billet temperatures exceed the nominal input due to adiabatic heating from plastic work inside a closed container. This has been experimentally studied by Sheppard et al. [32,33] and Lefstad et al. [34]. In Gleeble simulations, the much smaller sample volume significantly reduces adiabatic heating, leading to lower effective deformation temperatures. Thus, employing higher nominal temperatures in simulation provides a realistic approximation of the thermal state in the billet core during industrial extrusion. The comparison also highlights the inherent limitation of exit temperature measurements in industrial practice, which reflect surface conditions rather than the core. In addition to thermal effects, the strain-rate history in industrial extrusion is inherently non-uniform, evolving continuously along the deformation path [17] and the size effect also plays a role in laboratory scale simulations. In the present study, effective average value of 0.5/s agrees well with the texture comparisons in ODF (Fig. 6f and Fig. 4). Hence, the following sections will present a quantitative and detailed comparison between the industrially extruded sample and the physically simulated sample at 580 °C (T-580).

The microstructural analysis (Fig. 4 and Fig. 6) reveals a close correlation with both the samples. This supports the findings of Fylkesnes et al. [15] and Manik et al. [16] that the central region of a flat strip extrusion undergoes elongation along ED and thickness reduction along ND. The average grain thickness for the T-580 and extruded sample are measured out to be 2.41 ± 1.43 µm and 2.69 ± 1.48 µm. The volume fractions of LAGB and HAGB are presented in Fig. 7. The results shows that the T-580 sample has reduced LAGB fraction and higher HAGB fraction by a value of 13%. To further examine whether the elevated deformation temperature used in the physical simulation alters the deformation kinetics, a grain orientation spread (GOS) map comparison is performed and shown in Fig. 8. The fraction of recrystallised grains is comparable for both conditions, with the simulated sample showing only a marginal increase of approximately 1%. Instead, the T-580 condition exhibits a higher fraction of sub-structured grains by approximately 8% and a corresponding reduction in highly deformed grains relative to the industrial extrusion, indicating a modest enhancement of dynamic recovery. Both simulated and extruded microstructure shows the evidence of DRX grains which lead to the higher standard deviation values in the grain thickness. But nevertheless, the comparison reveals a good correlation.

The quantitative comparison of fibre textures and specific

**Table 1**
Quantitative measurement on the morphology and distribution of Fe based intermetallics for the extruded and the T-580 simulated sample.

| | Extruded | T-580 |
|---|---|---|
| **Avg. Area ($\mu m^2$)** | 1.81 ± 0.30 | 1.90 ± 0.17 |
| **Number Density ($\times 10^{-3}$ particles/$\mu m^2$)** | 3.7 ± 0.4 | 4.2 ± 0.1 |
| **Mean Aspect Ratio** | 0.46 ± 0.013 | 0.45 ± 0.010 |

orientation components further strengthens this validation (Fig. 7). The comparison reveals a strong correlation in the fibre texture distribution between the two samples. The dominant < 112>//ED fibre exhibits only a slight deviation showing a 8% higher volume fraction compared to the extruded sample. The < 111 > fibre remains consistent across both conditions, while the < 100 > fibre shows a reduction of approximately 8% in the simulated sample. The corresponding orientation components shown in Fig. 7 clarifies this observation. The Brass, S and cube components exhibit small differences of 5% in volume fraction with S component being a bit higher in the simulated sample and Cube, Brass component is slightly lower. Copper orientation stays almost consistent. The Goss component is minimal in both samples, and the CG 26.5 orientation shows good correlation. The texture index (J) of the T-580 sample is slightly higher than that of the industrially extruded reference, indicating a marginally strong overall texture intensity in simulation. Despite this difference, the dominant texture observed in industrial sample is well reproduced in the simulation.

The behaviour of Fe-based intermetallics provides an additional metric of validation. Fig. 8 compares the Fe-intermetallic particle size and shape distributions for both the extruded and the T-580 sample, with the corresponding quantitative values shown in Table 1. For transparency, one representative SEM image from each condition (Fig. 9a and b), along with its MATLAB based particle segmentation (Fig. 9c,d) and the resulting distributions is shown as an example. In both the conditions, the intermetallics are clearly fragmented from their original morphology (Fig. 3) and have become aligned along the ED with narrow aspect ratios (Fig. 9a). This indicates significant deformation and flow induced redistribution along the ED. A close agreement is observed, both in terms of intermetallic area distribution chart and the average area. In both cases the distributions are skewed towards the smaller sizes below 1 μm indicating extensive fragmentation. The aspect ratio distributions for both conditions exhibit a broad spread centred around similar mean values. The close agreement in the distribution spread and the quantitative measurements in the thermo-mechanical simulation with the industrial extrusion proves that the flow induced redistribution of Fe intermetallics along ED is accurately captured in the simulation.

To conclude, the thermo-mechanically simulated sample shows a close match with the industrial sample across all parameters. The close agreement in grain shape evolution between thermo-mechanical simulation and industrial extrusion confirms that the imposed strain path in the Gleeble test accurately reproduces the hot deformation mode of flat-strip extrusion. The plastic flow is accommodated by temperature-dependent slip activity and lattice reorientation, both of which govern texture development [35]. The successful replication of deformation and recrystallisation texture validates that the underlying mechanisms are realistically captured in the thermo-mechanical simulation. The observed minor quantitative differences in texture intensities between the simulated and industrial conditions may reasonably arise from the post deformation thermal exposure in the industrial extrusion (while travelling from die exit to quench tank) whereas in thermo-mechanical simulation, the sample is quenched immediately after deformation. Furthermore, the behaviour of second-phase particles provides an independent metric of deformation fidelity, since their fragmentation, alignment, and redistribution occur directly in response to material flow.

## 4. Summary

In the present work, a Gleeble based physical simulation methodology was developed to physically simulate the deformation conditions experienced in the central region of flat strip extrusion of an Al-Mg-Si-Cu alloy.

- The strain path in the billet core is identified as predominant compression along ND and elongation along ED from the literature

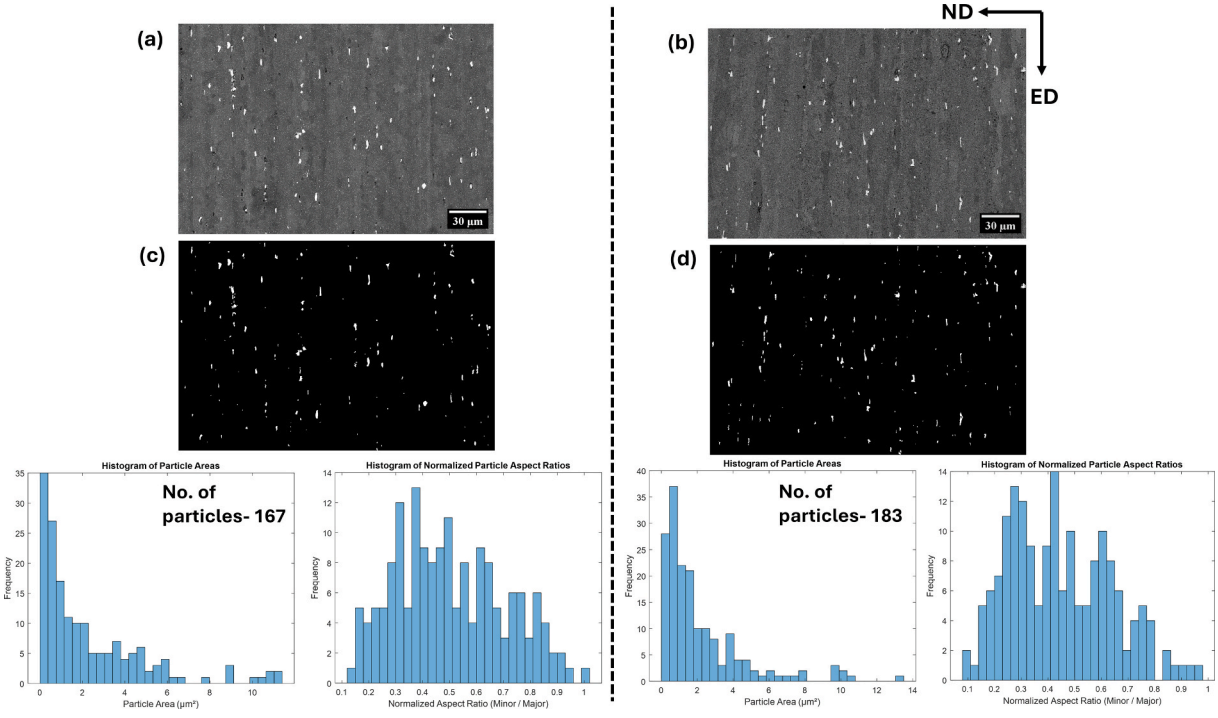


**Fig. 9.** SEM backscattered images of Fe based intermetallic particles in extruded (a) and T-580 (b).

and executed on small samples with the help of Gleeble under three different temperatures.

- The simulation necessitates 20 °C higher than actual industrial exit temperature range to accommodate industrial conditions. The executed strain path captured the key features of the process, including elongated, pancaked grains and the texture components characteristic of flat-strip extrusion.
- Despite a slight variation in grain boundary fractions (13%), the overall microstructural and texture agrees with industrial flat strip extrusion confirming the robustness of the thermo-mechanical simulation.
- Additionally, the consistent distribution and morphology of Fe intermetallic phases further confirm the reliability of the strain path used in the simulation.

The validation confirms that this modified plane strain method is a reliable tool for capturing the true deformation state of flat-strip extrusion. Beyond replication, it offers a versatile tool for exploring new alloy compositions, strain path effects, recrystallisation behaviour, and second-phase evolution. The methodology therefore enables extrusion to be approached not only as a shaping process but also as a route for deliberate microstructural design and process optimisation. Importantly, the ability to simulate extrusion conditions in a laboratory setting provides a cost-effective pathway for accelerating alloy development and optimising industrial extrusion processes.

## CRediT authorship contribution statement

**Sri Saran Gunasekaran:** Writing - original draft, Methodology, Validation, Investigation, Data curation, Formal analysis. **E. Bagherpour:** Writing – review & editing, Supervision, Conceptualization. **Chrysoula Tzileroglou:** Writing – review & editing, Validation, Supervision, Resources, Project administration, Conceptualization. **Carla Barbatti:** Writing – review & editing, Funding acquisition, Conceptualization. **Chamini L. Mendis:** Writing – review & editing, Validation, Supervision, Project administration, Methodology, Funding acquisition, Conceptualization.

## Declaration of competing interest

The authors declare that they have no known competing financial interests or personal relationships that could have appeared to influence the work reported in this paper.

## Acknowledgements

This research was funded by EPSRC (UK) under Industrial Case (ICase) studentship programme and Constellium UK. The authors would like to acknowledge the use of the BCAST Advanced Characterisation Suite (BACS) set up through the funding received from UKRI Infrastructure grant: entitled “Future Metallurgy Centre”.

## Appendix A. Supplementary data

Supplementary data to this article can be found online at https://doi.org/10.1016/j.matdes.2026.115724.

## Data availability

Data will be made available on request.

## References

[1] W.S. Miller, et al., Recent development in aluminium alloys for the automotive industry, Mater. Sci. Eng. A 280 (1) (Mar. 2000) 37–49, https://doi.org/10.1016/S0921-5093(99)00653-X.

[2] “(PDF) Electric vehicles spike demand for high strength aluminum extrusions.” Accessed: Aug. 03, 2024. [Online]. Available: https://www.researchgate.net/publication/328851054_Electric_vehicles_spike_demand_for_high_strength_aluminum_extrusions.

[3] Y. Wang, G. Zhao, X. Xu, X. Chen, Effect of extrusion parameters on microstructure, texture and mechanical property anisotropy of spray deposited 2195 Al–Li alloy profile, Mater. Sci. Eng. A 818 (2021) 141406, https://doi.org/10.1016/j.msea.2021.141406.

[4] X. Chen, G. Zhao, G. Liu, L. Sun, L. Chen, C. Zhang, Microstructure evolution and mechanical properties of 2196 Al-Li alloy in hot extrusion process, J. Mater. Process. Technol. 275 (Jan. 2020) 116348, https://doi.org/10.1016/J.JMATPROTEC.2019.116348.

[5] Y. Li, G. Zhao, L. Sun, B. Zhang, X. Zhao, Texture evolution induced by extrusion parameters and its effect on strengthening-toughening mechanisms of Al-Mg-Si-Cu-Mn alloys, Mater. Sci. Eng. A 916 (Nov. 2024) 147377, https://doi.org/10.1016/J.MSEA.2024.147377.

[6] L. Yang, H. Wang, Q. Shan, C. Qian, Z. Li, and H. Xiao, “Optimization of the Hot Extrusion Process for 6082 Aluminum Alloy W-Profile,” *J. Mater. Eng. Perform.*, pp. 1–13, Apr. 2025, doi: 10.1007/S11665-025-11203-8/FIGURES/13.

[7] J. Chen, “A study on the texture and microstructure development in extruded AA3003 alloys and the relevant mechanical behaviour,” 2018. [Online]. Available: https://open.library.ubc.ca/collections/24/items/1.0363888.

[8] T. Kayser, B. Klusemann, H.G. Lambers, H.J. Maier, B. Svendsen, Characterization of grain microstructure development in the aluminum alloy EN AW-6060 during extrusion, Mater. Sci. Eng. A 527 (24–25) (Sep. 2010) 6568–6573, https://doi.org/10.1016/J.MSEA.2010.06.050.

[9] A. Güzel, et al., A new method for determining dynamic grain structure evolution during hot aluminum extrusion, J. Mater. Process. Technol. 212 (1) (2012) 323–330, https://doi.org/10.1016/j.jmatprotec.2011.09.018.

[10] C. Zhang, C. Wang, Q. Zhang, G. Zhao, L. Chen, Influence of extrusion parameters on microstructure, texture, and second-phase particles in an Al-Mg-Si alloy, J. Mater. Process. Technol. 270 (Aug. 2019) 323–334, https://doi.org/10.1016/J.JMATPROTEC.2019.03.014.

[11] M. Araki, K. Matsuda, Effect of composition on recrystallization texture formation of aluminum extrusions, Mater. Trans. 61 (1) (2020) 104–110, https://doi.org/10.2320/MATERTRANS.MT-M2019226.

[12] M. Schikorra, L. Donati, L. Tomesani, A.E. Tekkaya, Microstructure analysis of aluminum extrusion: Prediction of microstructure on AA6060 alloy, J. Mater. Process. Technol. 201 (1) (2008) 156–162, https://doi.org/10.1016/j.jmatprotec.2007.11.160.

[13] A. Foydl, et al., Grain size evolution simulation in aluminium alloys AA 6082 and AA 7020 during hot forward extrusion process, Materials Science and Technology (united Kingdom) 29 (1) (Jan. 2013) 100–110.

[14] K. Zhang, K. Marthinsen, B. Holmedal, T. Aukrust, A. Segatori, Through thickness variations of deformation texture in round profile extrusions of 6063-type aluminium alloy: Experiments, FEM and crystal plasticity modelling, Mater. Sci. Eng. A 722 (Apr. 2018) 20–29, https://doi.org/10.1016/J.MSEA.2018.02.081.

[15] H. Fylkesnes and K. Zhang, “Texture and Microstructure Evolution during Extrusion of AlMgSi-Alloys,” *90*, 2016, Accessed: Jul. 03, 2024. [Online]. Available: https://ntnuopen.ntnu.no/ntnu-xmlui/handle/11250/2406967.

[16] T. Manik, K. Marthinsen, K. Zhang, A.I. Aria, B. Holmedal, Deformation Texture Evolution in Flat Profile AlMgSi Extrusions: Experiments, FEM, and Crystal Plasticity Modeling, Front. Mater. 8 (Mar. 2021) 636379, https://doi.org/10.3389/FMATS.2021.636379/BIBTEX.

[17] A. Zang, A. Khajezade, X. Wang, N. Parson, M. Wells, and W. J. Poole, “The Spatial Variation of Crystallographic Texture During Axisymmetric Solid Bar Extrusion of an Al–Mg–Si Alloy,” *Metall. Mater. Trans. A Phys. Metall. Mater. Sci.*, vol. 55, no. 4, pp. 1122–1136, Apr. 2024, doi: 10.1007/S11661-024-07309-8/TABLES/3.

[18] K. Zhang, K. Marthinsen, B. Holmedal, T. Aukrust, and A. Segatori, “EVOLUTION IN TEXTURE AND ITS THROUGH-THICKNESS VARIATIONS IN Al-Mg-Si-EXTRUSIONS: EXPERIMENTS AND MODELLING”.

[19] T. Aukrust, S. Tjøtta, H.E. Vatne, P. Van Houtte, Coupled FEM and texture modelling of plane strain extrusion of an aluminium alloy, Int. J. Plast 13 (1–2) (Jan. 1997) 111–125, https://doi.org/10.1016/S0749-6419(97)00003-X.

[20] K. Zhang, K. Marthinsen, B. Holmedal, T. Aukrust, A. Segatori, Coupled FEM and Alamel-type Polycrystal Plasticity Modelling Applied to Extrusion of Aluminium Alloys, Mater. Today Proc. 2 (10) (2015) 4898–4903, https://doi.org/10.1016/J.MATPR.2015.10.049.

[21] F. Parvizian, T. Kayser, B. Klusemann, B. Svendsen, Modelling and simulation of dynamic microstructure evolution of aluminium alloys during thermomechanically coupled extrusion process, Int. J. Mater. Form. 3 (SUPPL. 1) (Apr. 2010) 363–366, https://doi.org/10.1007/S12289-010-0782-4/METRICS.

[22] M. Zhou, C. Tzileroglou, C. Barbatti, H. Assadi, Novel texture analysis method for optimising material property in extruded 6xxx alloys using artificial neural networks, Mater Charact 223 (May 2025) 114859, https://doi.org/10.1016/J.MATCHAR.2025.114859.

[23] Q. Zhao, Z. Liu, Texture Evolution of Hot rolled Al–Cu–Mg–Zr Alloy during Annealing, Met. Mater. Int. 28 (12) (Dec. 2022) 2947–2961, https://doi.org/10.1007/S12540-022-01186-9/FIGURES/12.

[24] R. Kumar, A. Gupta, T.R. Dandekar, R.K. Khatirkar, Microstructure and texture development in AA3003 aluminium alloy, Mater. Today Commun. 24 (Sep. 2020) 100965, https://doi.org/10.1016/J.MTCOMM.2020.100965.

[25] P.S. Bate, Y. Huang, F.J. Humphreys, Development of the ‘brass’ texture component during the hot deformation of Al–6Cu–0.4Zr, Acta Mater. 52 (14) (Aug. 2004) 4281–4289, https://doi.org/10.1016/J.ACTAMAT.2004.05.044.

[26] E. Harma, P. Sanders, T. Wood, and T. Langan, "The Influence of Extrusion Geometry and Ratio on Extrudate Mechanical Properties for a 6005A Alloy Containing Either Sc and Zr or Cr and Mn Dispersoid Formers," *Journal of Manufacturing and Materials Processing 2025, Vol. 9, Page 168*, vol. 9, no. 5, p. 168, May 2025, doi: 10.3390/JMMP9050168.

[27] A. Brahme, C.L. Park, J. Tschirhart, A. Lakshmanan, S. Das, K. Inal, Towards optimizing the thermal processes in aluminum alloys using a full-field CA based approach for static recrystallization modeling, J. Mater. Res. Technol. 35 (Mar. 2025) 2946–2954, https://doi.org/10.1016/J.JMRT.2025.01.220.

[28] "(PDF) Physical simulation of metallurgical processes." Accessed: Aug. 27, 2025. [Online]. Available: https://www.researchgate.net/publication/289726847_Physical_simulation_of_metallurgical_processes.

[29] C. Slater, N. Tamanna, and C. Davis, "Optimising compression testing for strain uniformity to facilitate microstructural assessment during recrystallisation," 2021, doi: 10.1016/j.rinma.2021.100218.

[30] C.-Q. Huang and L. Liu, "Application of the Constitutive Model in Finite Element Simulation: Predicting the Flow Behavior for 5754 Aluminum Alloy during Hot Working," *Metals (Basel).*, vol. 7, no. 9, 2017, doi: 10.3390/met7090331.

[31] C. Poletti, R. Bureau, P. Loidolt, P. Simon, S. Mitsche, and M. Spuller, "Microstructure Evolution in a 6082 Aluminium Alloy during Thermomechanical Treatment," *Materials 2018, Vol. 11, Page 1319*, vol. 11, no. 8, p. 1319, Jul. 2018, doi: 10.3390/MA11081319.

[32] I. Flitta, T. Sheppard, Effect of pressure and temperature variations on FEM prediction of deformation during extrusion, Mater. Sci. Technol. 21 (3) (Mar. 2005) 339–346, https://doi.org/10.1179/174328405X29221;PAGE:STRING:ARTICLE/CHAPTER.

[33] T. Sheppard, Temperature changes occurring during extrusion of metals: Comparison of bulk, numerical, and integral profile predictions with experimental data, Mater. Sci. Technol. 15 (4) (1999) 459–463, https://doi.org/10.1179/026708399101505941.

[34] M. Lefstad and O. Reiso, "Temperature Measurements in Extrusion Dies," *Materials Science Forum*, vol. 217–222, no. PART 1, pp. 409–414, 1996, doi: 10.4028/WWW.SCIENTIFIC.NET/MSF.217-222.409.

[35] H. J. McQueen, *Hot deformation and processing of aluminum alloys*. CRC Press, 2011. Accessed: Jul. 08, 2024. [Online]. Available: https://www.routledge.com/Hot-Deformation-and-Processing-of-Aluminum-Alloys/McQueen-Spigarelli-Kassner-Evangelista/p/book/9781138071636.